Substituents' effect on the photophysics of trinuclear copper(I) and silver(I) pyrazolatephosphine cages

Kristina F Baranova, Aleksei A Titov, Julia R Shakirova, Vadim Baigildin, Alexander F Smol'Yakov, Dmitry A. Valyaev, Guo-Hong Ning, Oleg A Filippov, Sergey P Tunik, Elena S Shubina

Substituents' effect on the photophysics of trinuclear copper(I) and silver(I) pyrazolate-phosphine cages

Kristina F. Baranova,[‡] Aleksei A. Titov,[‡] Julia R. Shakirova,[§] Vadim Baigildin,[§] Alexander F. Smol'yakov,[‡‖] Dmitry A. Valyaev,[⊥] Guo-Hong Ning,[#] Oleg A. Filippov,[‡] Sergey P. Tunik,[§]* and *Elena S. Shubina[‡*]*

[‡] *A. N. Nesmeyanov Institute of Organoelement Compounds, Russian Academy of Sciences, Vavilov Str., 28, 119991 Moscow, Russia*

[§] *Institute of Chemistry, St. Petersburg State University Universitetskii pr., 26, 198504, St. Petersburg, Russia*

[‖] *Plekhanov Russian University of Economics, Stremyanny per. 36, 117997, Moscow, Russia.*

[⊥] *LCC−CNRS, Université de Toulouse, CNRS, 205 route de Narbonne, 31077 Toulouse Cedex 4, France*

[#]*`Department College of Chemistry and Materials Science, Guangdong Provincial Key Laboratory of Functional Supramolecular Coordination Materials and Applications Jinan University, Guangzhou, Guangdong 510632, P. R. China*

KEYWORDS

copper(I) complex, silver(I) complex, coinage metals, cyclic pyrazolate complex, photoluminescence, TADF, TD-DFT

ABSTRACT

A series of structurally similar trinuclear macrocyclic copper (I) and silver (I) pyrazolate complexes bearing various short-bite diphosphine $R_2PCH(R')PR_2$ ligands are reported. Upon diphosphine coordination the planar geometry of the initial complexes undergoes bending along the line between two metal atoms coordinated to the phosphorus moieties. The complexes based on dcpm ligands (R = cyclohexyl, R' = H, Ph) do not exhibit dynamic behavior in solution at room temperature on ^{31}P NMR time scale as it was previously observed for similar trinuclear copper complexes bearing dppm (R = Ph, R' = H) scaffold. All copper (I) complexes exhibit TADF behavior in the solid state. Importantly, the use of aliphatic substituents on the phosphorous atoms instead of aromatic ones leads to almost double increase in the quantum efficiency (Φ_{PL}) of photoluminescence by eliminating non-radiative decay from the $^3LC^{Ph}$ states of the dppm aromatic rings. Higher donating ability of the substituents in the pyrazolate ligand (CF_3 *vs.* CH_3) lowers the energy of the metal-centered excited state, allowing for a significant metal impact into the T_1 state. Finally, Ag(I) complex displays an emission efficiency of approximately 14% being the highest among known trinuclear silver(I) pyrazolate homometallic derivatives.

INTRODUCTION

A considerable interest to the chemistry of luminescent copper and silver complexes[1-3] is sustained by their high emission quantum yields, low cost, and environmentally friendly properties thus making them highly promising objects for a wide range of applications in electroluminescent devices (OLEDs and LECs),[4-9] photocatalysis,[10-13] and dye-sensitized solar cells.[14-16] Typically, the Cu(I) complexes supported with N-coordinating ligands and ancillary phosphine donors exhibit photoluminescence from the metal-to-ligand charge transfer (MLCT) excited state.[17] In contrast, Ag(I)-containing analogues typically do not exhibit the participation of metal ions in charge transfer due to their higher oxidation potentials and display ligand-centered (LC) emission. The large spin-orbit coupling (SOC), caused by the presence of heavy silver atoms, leads to the phosphorescence originated from the mixing of singlet and triplet excited states.[18-19] However, for some silver(I) complexes particular ligand environment can favor an emission from excited states with charge-transfer character (MLCT or ILCT)[20-24] similar to the phosphorescence behavior of copper(I) complexes.[25-27] Since MLCT excited states of d^{10} metal complexes can have a small energy gap between the S_1 singlet and T_1 triplet states, the equilibrium between them at room temperature becomes possible resulting in long-lived emission called thermally-activated delayed fluorescence (TADF).[20, 28-33] In the latter case, harvesting both triplet and singlet excitations represents one of the main advantages of such complexes that can be used for the fabrication of efficient electroluminescent devices. [29, 34, 35-36]

Trinuclear coinage metal pyrazolates attract considerable interest due to their versatile coordination chemistry and intriguing photoluminescence properties.[37-39] Recently, we have demonstrated that the adducts of trinuclear copper(I) pyrazolates with bis(diphenylphosphino)methane (dppm) exhibit TADF behavior.[40] The variation of the substituents in pyrazole moiety or coordination of additional ligands to the metal core allow the

modulation of emission characteristics in a wide range of spectral parameters, lifetimes, and efficiency.[41-43] Acting as Lewis acids, trinuclear d^{10} metal pyrazolates form stable adducts with the bases of different nature.[44-49] It was also shown that solid-state photophysics of the trinuclear Cu(I) pyrazolates can also be influenced by weak intermolecular interactions.[50-52] Furthermore, short intermolecular metal-metal contacts in crystal cell may provide electronic communication between the metal cores leading to formation of exciplexes upon photoexcitation.[53] The substituents in pyrazolate ligand affect the possibility of the complexes stacking, resulting in various modes of M···M interactions and supramolecular packing that considerably modulate solid state luminescence.[54]

As we have previously shown, dppm may serve as a bridging ligand linking two metals in cyclic trinuclear pyrazolates without destruction of the central M_3N_6 core and ensure the additional stabilization of a whole molecule.[40] These Cu(I) and Ag(I) diphosphine adducts display the same structural features and substantially modified photophysical behavior compared to the starting compounds with the negative effect of the phenyl substituents at the dppm, which increase a contribution of non-radiative decay channels into excited state relaxation. Obviously, further modulation of the photophysical parameters for this type of emitters may be achieved by the variations in donor properties of the diphosphine ligands and electronic characteristics of the components of central core, which both take active part in emissive transitions. The latter can be done by introduction of donor/acceptor substituents in the pyrazolate ligands to change the properties of the $[ML]_3$ system.

Herein we present synthesis, structural characterization, photophysical and theoretical studies for a new series of macrocyclic trinuclear copper(I) and silver(I) complexes bearing various combinations of pyrazolate and diphosphine ligands (Scheme 1).

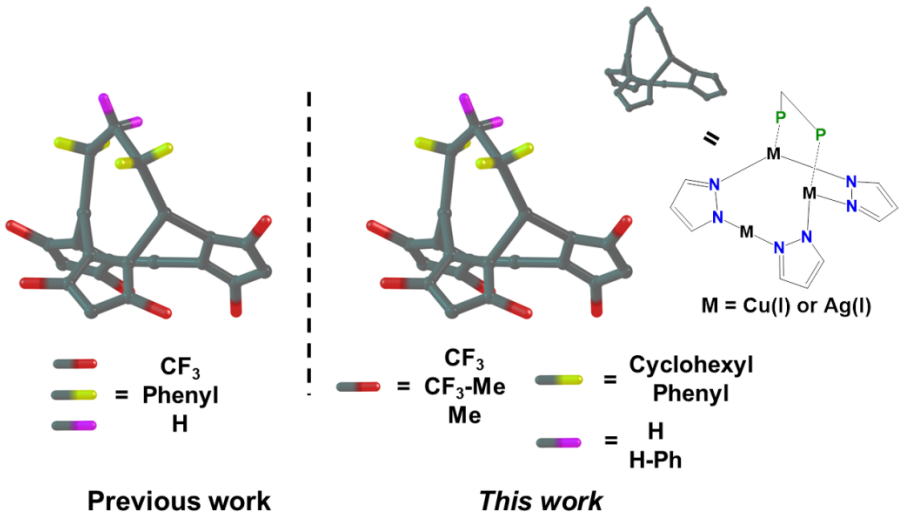

Scheme 1. A schematic representation of the complexes used in the previous[40] and current study.

RESULTS AND DISCUSSION

Copper(I) and silver(I) pyrazolate adducts **1-8** (Scheme 2) were prepared by the reaction of equimolar amounts of cyclic trinuclear complexes $[ML^n]_3$ (L^1 = 3,5-$(CF_3)_2$Pz; L^2 = 3-CH_3-5-CF_3-Pz; L^3 = 3,5-$(CH_3)_2$Pz) and the corresponding diphosphines in toluene. The reaction products are readily soluble in common organic solvents (CH_2Cl_2, $CHCl_3$, benzene, acetone, and boiling hexane). All compounds have been characterized by elemental analysis, FTIR and NMR spectroscopy (see Experimental section and Figures S1-S25 in the Supporting Information) that confirmed the formation of the products in 1:1 stoichiometric ratio, see Scheme 2.

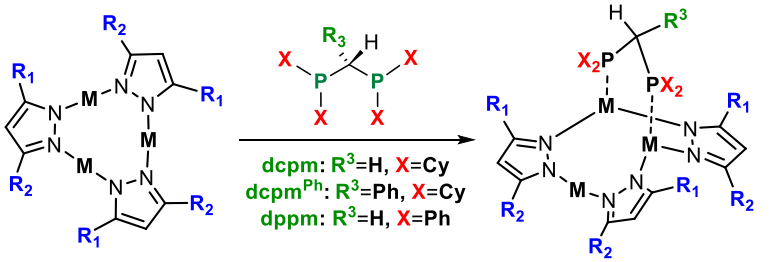

$[CuL^1]_3$: M=Cu(I), R^1=R^2=CF_3 1: {$[CuL^1]_3$(dcpm)}; 2: {$[CuL^1]_3$($dcpm^{Ph}$)}
$[AgL^1]_3$: M=Ag(I), R^1=R^2=CF_3 3: {$[AgL^1]_3$(dcpm)}; 4: {$[AgL^1]_3$($dcpm^{Ph}$)}
$[CuL^2]_3$: M=Cu(I), R^1=CF_3, R^2=CH_3 5: {$[CuL^2]_3$(dcpm)}; 6: {$[CuL^2]_3$(dppm)}
$[CuL^3]_3$: M=Cu(I), R^1=R^2=CH_3 7: {$[CuL^3]_3$(dcpm)}; 8: {$[CuL^3]_3$(dppm)}

Scheme 2. Chemical structure of copper(I) and silver(I) pyrazolate adducts **1**-**8** unveiled in this work

In the case of complexes **1**, **3**, **5**, **7** bearing the $Cy_2PCH_2PCy_2$ (dcpm) ligand, the ^1H resonance of the methylene bridge cannot be unambiguously detected due to overlapping with the signals of protons in cyclohexyl fragments. In contrast, the signal of the bridging proton of coordinated $Cy_2PCH(Ph)PCy_2$ ($dcpm^{Ph}$) in complex **2** can be easily distinguished and appears as a triplet at δ_H 3.82 with $^2J_{PH}$ coupling of 10.5 Hz. Similar chemical shift was also found in Ag(I) complex **4** albeit in this case additional coupling with $^{107/109}$Ag nuclei was observed. Silver-containing complexes **3-4** show resolved $^{31}P\{^1H\}$ NMR multiplets, due to coupling with $^{107/109}$Ag isotopes. These spectroscopic patterns are essentially similar to those observed for the $\{[AgL1]_3(dpcm)\}$ complex at 198K,[40] suggesting the absence of "merry-go-round" motion of the dcpm ligand around the Ag_3 core in the ^{31}P NMR timescale at room temperature contrary to the rapid movement of dppm about the same Ag_3 core.[40] This observation can be rationalized by the higher donating ability of the dcpm ligand compared to dppm, resulting in a stronger M-P bond formation that agrees with DFT calculations (see Table S1 in Supporting Information). The obtained ^1H and ^{31}P NMR spectra demonstrate the number of signals, their multiplicity, and relative intensities, which are consistent with the overall structural pattern depicted in Schemes 1 and 2.

Solid State Structure Determination

Crystals of complexes **1-4**, **6**, and **7** suitable for single-crystal X-ray diffraction analyses, were obtained by crystallization from a CH_2Cl_2/hexane solution. All complexes retain the central nine-membered M_3N_6 core with significant distortions from the planar geometry of the original cyclic trinuclear metal pyrazolate adducts. The starting planar metallacycle bends along the line

connecting the metal atoms coordinated to the diphosphine ligand, as was previously observed for analogous {[ML^1]$_3$(dppm)} complexes (**Figure 1**).[40] Selected bond lengths and angles are listed in **Table 1.** A comparison of the bond lengths found in the copper-containing complexes **1**, **2**, **6**, and **7** with those obtained earlier for the {[CuL^1]$_3$(dppm)} (**1***) structure[40] shows the essential similarity in these structural parameters. The variations in angular characteristics observed in these compounds are also insignificant and are likely due to differences in the steric effects of the coordinated diphosphines.

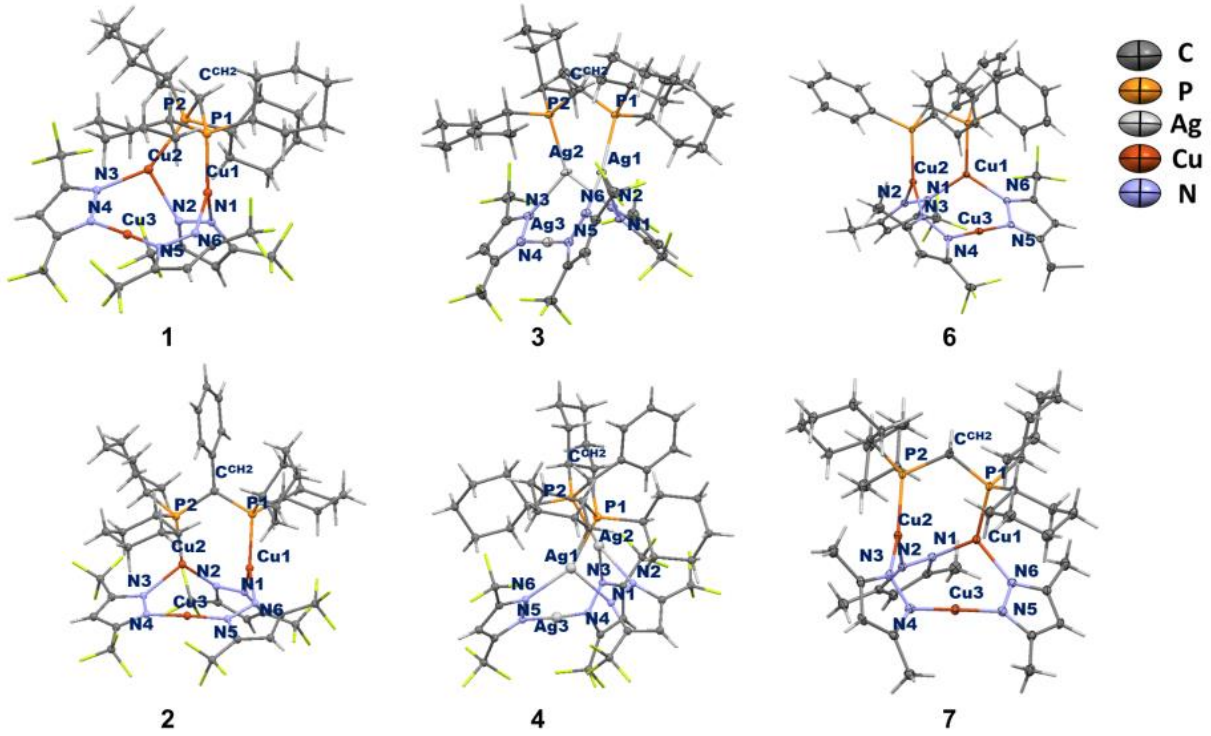

Figure 1. XRD structures of complexes **1-4**, **6**, **7** with thermal ellipsoids set at 30% probability level. Hydrogen and fluorine atoms are shown as sticks for clarity.

In turn, silver complexes, having stronger M−P interactions than their copper analogues, exhibit larger macrocycle bending. Increasing diphosphine ligand donicity led to further distortion of the M_3N_6 core. The Ag…P bond lengths are comparable for complexes **3**, **4** and

previously described {[AgL[1]]$_3$(dppm)} (**3***) (2.3363(6)-2.3985(6) Å).[40] The observed distortions correlate well with notable variations in the lengths of the Ag-N bonds (2.1848(1)-2.503(1) Å) in the structural fragment containing the Ag1−N1−N2−Ag2 pyrazolate bridge. The coordination of the phosphorus atoms leads to significant folding of the Ag_3N_6 plane, resulting in the appearance of short intramolecular contacts Ag3…N1 of 2.960(1) and 2.795(2) Å in **3** and **4**, respectively (**Figure 2**).

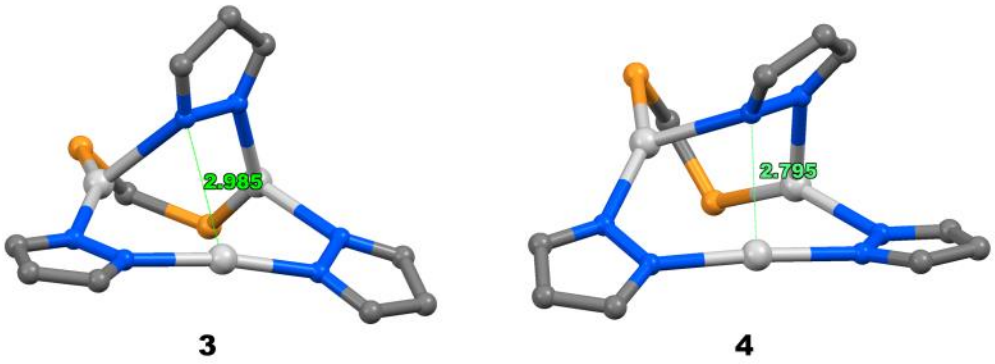

Figure 2. [AgL]$_3$(PCP) fragments of complexes **3** and **4** demonstrating intramolecular N^{Pz}…Ag distances.

Table 1. Selected bonds lengths and angles in **1-4**, **6-7** and previously published complexes **1*** and **3***.[40]

	M1-P1	M2-P2	∠N1-M1-N6	∠N2-M2-N3	∠N4-M3-N5	Bending angle[a]
1	2.189	2.211	103.4	98.7	175.0	83.5
2	2.207	2.202	105.3	110.4	177.6	77.1
6	2.187	2.185	112.2	106.4	177.9	84.2
7	2.163	2.205	106.0	101.8	175.9	86.9
1*	2.175	2.200	104.7	104.8	177.2	86.6
3	2.374	2.347	90.0	94.6	173.0	75.2
4	2.396	2.364	101.4	84.9	175.1	74.2
3*	2.336	2.373	92.6	92.2	175.7	75.8

[a] the angle between M1M2N3N4M3N5N6 and M1N1N2M2 planes

Photophysical studies

Copper(I) complexes **1**, **2**, **5-8** luminesce in solution and in solid state, whereas the silver compounds **3** and **4** are non-emissive in solution. Photophysical characteristics of the emissive complexes are summarized in **Table 2** and 3, their absorption, excitation and emission spectra are shown in Figure 3, S24-S31 (see the Supporting Information). In deaerated dichloromethane solution at room temperature, the copper complexes **1**, **2** and **5-8** display rather weak green phosphorescence (λ_{em} varies from 525 to 537 nm) with monoexponential emission decay and the lifetimes in the range 0.11-1.22 μs (Table 2), similar to the studied earlier Cu(I) dppm analogues.[40] The emission occurs from the excited state of the mixed ^{3}MLCT+^{3}LLCT character analogously to the close relatives[40, 55] and shows a small red shift of emission bands (7-22 nm) upon cooling down to 77K.

Table 2. Photophysical properties of Cu(I) complexes (**1**, **2**, **5-8**) in CH_2Cl_2 solution.

	T/K	λ_{abs}/nm ($\varepsilon \times 10^{-3}$, $cm^{-1}M^{-1}$)	λ_{exc}/nm[a]	λ_{em}/nm	τ[c] (aer/deaer)/ μs
1	298[c]	233(*31*), 300[sh](*2*)	301	527	0.22/0.55
	77[b]		319	535[b]	
2	298[c]	232(*39*), 300(*2.6*)	325	525	0.47/1.22
	77[b]		280[sh], 301	542[b]	
5	298[c]	236(*30*), 300(*1.6*)	296, 360	528	0.13/0.24
	77[b]		294[sh], 316, 376[sh]	542[b]	
6	298[c]	230(*37*), 264s[h](*14*), 325(*2.5*)	367	533	0.19/0.60
	77[b]		297, 337	540[b]	
7	298[c]	238(*37*), 320(*1.4*)	358	537	0.05/0.11
	77[b]		280[sh], 323, 338	559[b]	

8	298[c]	238(*41*), 270sh(*10*), 340(*0.7*)	311, 355	533	0.06/0.36
	77[b]		284, 332	545[b]	

a) Excitation spectra are measured at emission maxima; b) λ_{ex} = 320 nm; c) emission lifetimes were measured at the corresponding emission maxima, λ_{ex} = 355 nm; sh - shoulder

In the solid state the copper complexes exhibit strong emission and high values of the photoluminescence lifetime ranging from tens to hundreds of microseconds, see Table 3 and Figures 3, S26-S30. The position of emission maxima shows dependence on the temperature and the substituents in the pyrazolate and phosphine ligands. Similar to the behavior of these compounds in solution, they display a red shift of emission upon the samples cooling down to 77K, however, the temperature effects in solid state are stronger to give the bathochromic shift up to 55 nm (1982 cm^{-1}) in the case of **2**. The silver(I) pyrazolate adducts **3** and **4** exhibit appreciable blue emission (Table 3). It should be noted, that the silver complex **3** exhibits blue emission with the maximum at 420 nm with Φ_{PL} of 14% being to the best of our knowledge the highest value ever reported for the Ag-pyrazolate systems.

Table 3. Photophysical properties of **1-3**, **5-8** in solid state at 295 and 77K.

	M	Substituents R_1/R_2	Phosphine	T/K	λ_{exc}/ nm[a]	[a]λ_{em}/ nm	[b]τ/[d] µs	[e]Φ_{PL}/ %	[f]k_r, s^{-1}	[g]k_{nr}, s^{-1}
1	Cu	CF_3/CF_3	dcpm	295	302	513	60	72	1.2×10^4	0.5×10^4
				77	293[sh], 308	557	203		–	
2	Cu	CF_3/CF_3	$dcpm^{Ph}$	295	308	500	52	39	7.5×10^3	1.2×10^4
				77	305	555	257		–	
3	Ag	CF_3/CF_3	dcpm	295	218, 318[sh]	427	40	14	3.6×10^4	2.2×10^4
				77	273, 318	436	78.0[c]		–	
5	Cu	CF_3/CH_3	dcpm	295	283[sh], 319	515	23	58	2.5×10^4	1.8×10^4
				77	270[sh], 316	565	215		–	
6	Cu	CF_3/CH_3	dppm	295	294[sh], 339, 356[sh]	520	18	72	4.0×10^4	1.5×10^4
				77	292, 339	570	129		–	
7	Cu	CH_3/CH_3	dcpm	295	298[sh], 332		42	74	1.9×10^4	0.7×10^4
				77	285[sh], 323	551	142.2		–	
8	Cu	CH_3/CH_3	dppm	295	306[sh], 356		15	58	3.8×10^4	2.8×10^4
				77	297[sh],344	585	116.5		–	

a) Excitation spectra are measured at emission band maxima; b) emission lifetimes were measured at the corresponding emission maxima, λ_{ex} = 355 nm; c) λ_{ex} was 263 nm; d) the measurement uncertainty of 5%; e) measurement uncertainty of 10%; f) $k_r = \frac{\Phi}{\tau}$; g) $k_{nr} = \frac{1-\Phi}{\tau}$.

The solid-state emission spectra are shown in Figure 3 and have been grouped to make possible a clear comparison of the effects induced by the nature of the ligands substituents. The variations in the emission bands maxima observed at room temperature are not essential in most cases, λ_{em} fall in the range from 510 to 533 nm (see Table 3 and panels A, B, C. E in Figure 3), whereas at 77K these effects are more pronounced. The observed effects may be summarized in the following way:

1) Analysis of the data presented in Figures 3A (dppm adducts), where pyrazolate ligands contain two CF_3, CH_3 and CF_3, and two CH_3 substituents (1*→6→8), shows that this group of emitters displays a systematic blue shift of emission wavelength upon introduction of CF_3 substituents in pyrazolate ligands both at room and low temperature. This observation is in line with the major contribution of ^{3}MLCT (metal→dppm)[39] into the lowest excited states. Electron withdrawing substituents in pyrazolates give a considerable decrease in the energy of metal centred orbitals and increase in the energy gap with the introduction of electron withdrawing groups into pyrazolate rings.
2) At the same time the dcpm-containing complexes (Figure 3B) do not display a systematic trend in emission maxima wavelengths upon introduction of electron withdrawing substituents into pyrazolates. This observation is not surprizing taking into account the change in the nature of the lowest energy transitions, which display predominant MC character, *vide infra*, in this class of complexes. Variations in donor ability of pyrazolates affect the energy of both ground and excited state orbitals to give smaller and less predictable effects.
3) In the series of complexes with two CF_3 substituents in pyrazolate rings, the variations in the nature of substituents at the bridging carbon atom of the diphoshine only slightly affect emission wavelengths (Figure 3C), evidently due to remote location of this moiety with respect to the orbitals taking part in emissive transitions. The only observable effect is a weak hypsochromic shift of emission maximum of **2** in comparison with **1** in room temperature spectra.
4) For the complexes containing two CF_3 and CF_3/CH_3 groups in pyrazolate ligands the variations in the substituents at the diphosphine ligands (Ph↔Cy) do not display any

significant effect onto the position of emission band maxima (Figure 3C and 3D). The nature of lowest energy transitions for the complexes containing diphosphines with Ph and Cy groups is very different, MLCT and MC, respectively, that complicates direct comparison between these types of chromophores.

5) However, in the case of the complexes with CH_3 substituted pyrazolates (Figure 3E) one can observe a considerable blue shift of emission wavelength for the complex with cyclohexyl substituted diphosphine that indicates higher energy gap for this chromophore compared to the complex with dppm ligand.
6) Analysis of the excited state relaxation constants (k_r and k_{nr}, Table 3), showed that their values are of the same order of magnitude for all complexes studied and do not display any systematic trends upon variations in electronic characteristics of both pyrazolate and diphosphine ligands. This observation is not surprizing because dynamic characteristics of excited state in solid samples are determined by a complicated combination of the influence of molecular electronic structure and intermolecular interactions in crystal cell, which may either compensate or enlarge the experimentally observed effects.

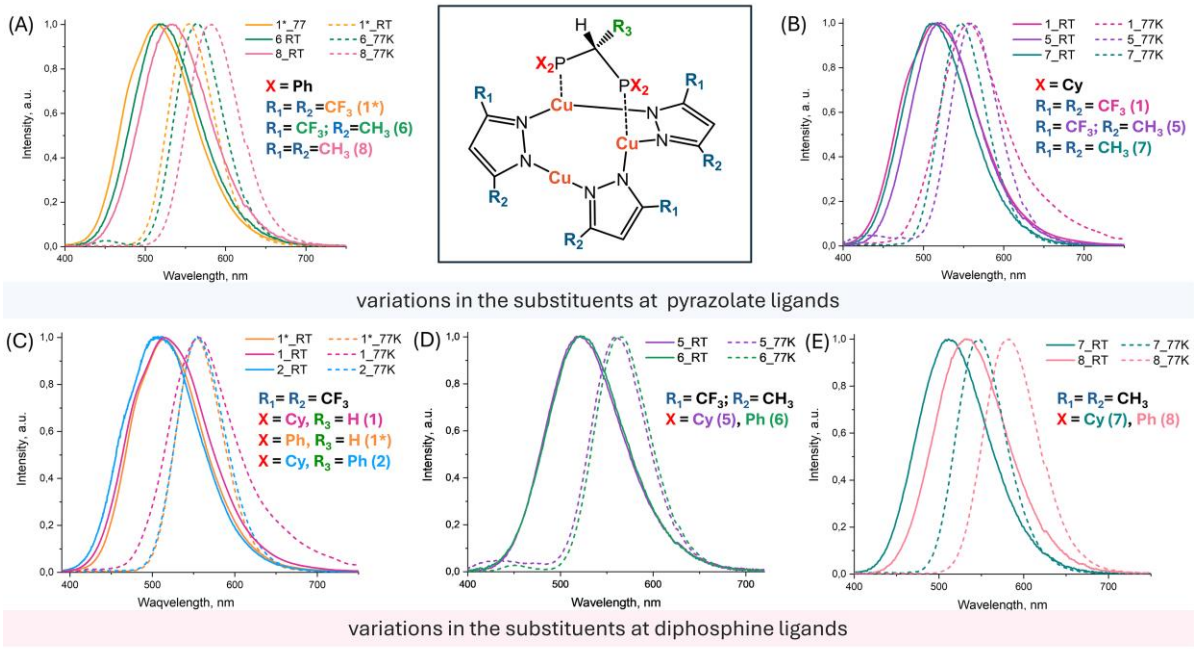

Figure 3. Solid-state emission spectra of copper **1**, **2**, **5-8** complexes at 298 and 77 K.

However, the most important features of the copper complexes photophysics in the solid state deal with emission bands red shift upon cooling the samples down to 77K, that is accompanied by sharp growth of emission lifetime (up to 257 μs for the complex **8**), and sigmoid lifetime dependence on temperature, see Table 3, Figure 4, S26-S30. This type thermochromic behaviour is typical for the mono-, di- and polynuclear copper complexes, which display TADF emission.[28, 30, 33, 56-59]

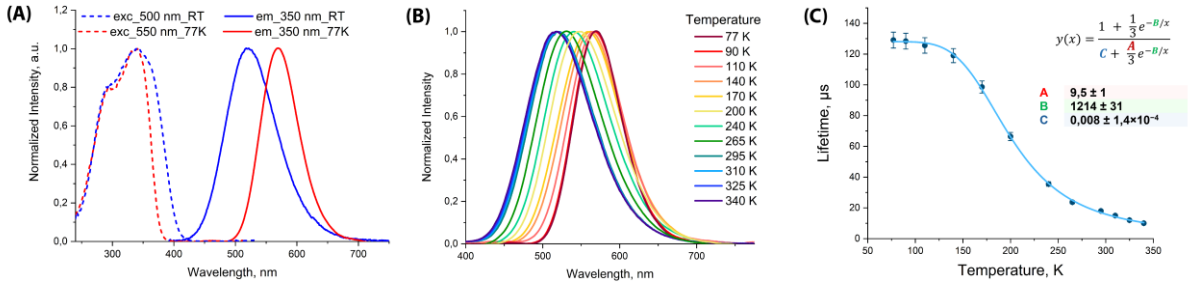

Figure 4. (A) Solid state excitation and emission spectra of **6**. (B) Temperature dependence of normalized emission spectra of 7. (C) Emission lifetimes variations in in the range 77-340K.

To get a deeper insight into the nature of the observed photophysical behaviour of the studied copper complexes the thermochromic characteristics of **1**, **2, 5-8** has been studied in detail including numerical simulation of the lifetime temperature dependence. Temperature variations of emission lifetimes for these complexes (Figure 4C, S29-S34) display the sigmoid curves, which can be fitted using a standard equation 1.[56 40]

$$\tau(obs) = \frac{1+\frac{1}{3}\exp(-\frac{\Delta E_{ST}}{k_B T})}{\frac{1}{\tau(T_1)}+\frac{1}{3\tau(S_1)}\exp(-\frac{\Delta E_{ST}}{k_B T})} \qquad \text{(Eq. 1)}$$

The data treatment with Eq. 1 gives the lifetimes of the lowest singlet $\tau(S_1)$ and triplet $\tau(T_1)$ along with the energy difference between these states $\mathbf{\Delta E_{ST}}$; the obtained parameters are summarized in **Table 4**. The temperature dependence of emission parameters for the copper-containing complexes is entirely compatible with the TADF mechanism of excited state relaxation. Indeed, the bathochromic shift of emission wavelength upon cooling the solid state copper complexes to a low temperature limit (77K and below) means predominant the population of the emissive triplet state, which is responsible for the extremely long emission lifetime of a hundred microseconds order under these conditions. Upon sample warming, one can observe a reduction of emission lifetime that is dictated by the population of higher lying S_1 state and the growing contribution of fluorescence into the observed emission. It proved to be impossible to reach the high temperature limit plateau in the τ vs T coordinate (Figures S26-S30) because of the complexes' decomposition at the temperature above 370K. Nevertheless, the energy gap between equilibrated singlet and triplet states can be calculated by using Eq. 1; see

Table 4. Excited states characteristics of **1**-**2**, **5**-**8** in solid state derived from equation 1.

Complex	$\tau(S_1)$, μs	$\tau(T_1)$, μs	$\Delta E_{ST,}$ cm^{-1}	ΔE_{ST}, eV
1	0.55±0.05	204±20	823±82	0.10±0.01
2	0.38±0.04	254±25	831±83	0.10±0.01
5	0.11±0.01	210±21	895±89	0.11±0.01
6	0.11±0.01	128±12	847±85	0.11±0.01
7	0.25±0.03	141±14	871±87	0.11±0.01
8	0.14±0.02	117±12	742±74	0.09±0.01

Photophysical properties of silver complex **3** also closely resemble "classic" TADF behavior (Figure S30) namely a bathochromic shift of the emission upon cooling and sigmoid temperature dependence. However, numerical analysis of the lifetime *vs* temperature curve and obtaining reliable magnitudes of the fluorescence and phosphorescence lifetimes and ΔE_{ST} values is impossible due to the thermal instability of the silver compounds that prevent measurements at the temperatures close to the high temperature plateau of the corresponding plots, in particular, the uncertainty in determination of $\tau(S_1)$ is more than 100% (calculation results given in Figure S34).

TD-DFT calculations

The TD-DFT calculations were performed by ωB97X-D3 with ZORA-def2-TZVPP basis set (SARC-ZORA-TZVPP basis set was applied for silver atoms) in CH_2Cl_2 introduced by CPCM model. We observed the same metal-centered (MC) excited states for all complexes. It consists of electron density transfer from two phosphorous-bonded metal atoms, with a larger contribution from one of them to the excited state (electron), spread between all three metal atoms, each contributing 10-20%. The pyrazolate ligands contribute approximately 20% to both

the hole and the electron (Table S3). For the Cu(I) complexes with dcpm phosphine, MC state identified as both S_1 and T_1 state with a >89% fractions (Figure 5 left), while for the silver compounds, it is the lowest excited state for singlets and could be localized by NTO analysis in T_3 (0.1 fractions) and T_4 (0.65 fractions) states (Figure 5 right). Based on the TD DFT analysis, we hypothesize that for the Ag complex **3**, there should be mostly LC^{Pz}-based phosphorescence from the doubly degenerated T_1/T_2 states, whereas the reversible intersystem crossing (RISC) process is obstructed by both low $<S_1|T_1>$ spin-orbit coupling and high singlet-triplet energy gap. Moreover, complex **3** possesses low SOC $<S_1|T_x>$ values for the excited triplets up to T_7 (SOC < 32 cm^{-1}). Copper complexes demonstrate simpler behavior: the lowest singlets and triplets are of MC nature, characterizing by rather high SOC's $<S_1|T_1>$ values. It is worth noting that the dppm complex **8** has a maximal $<S_1|T_1>$ SOC value (276 cm^{-1}), while for dcpm complexes **1** and **7,** we could expect alternative $<S_1|T_2>$ or $<S_2|T_1>$ RISC pathways based on the SOC values (Table 5).

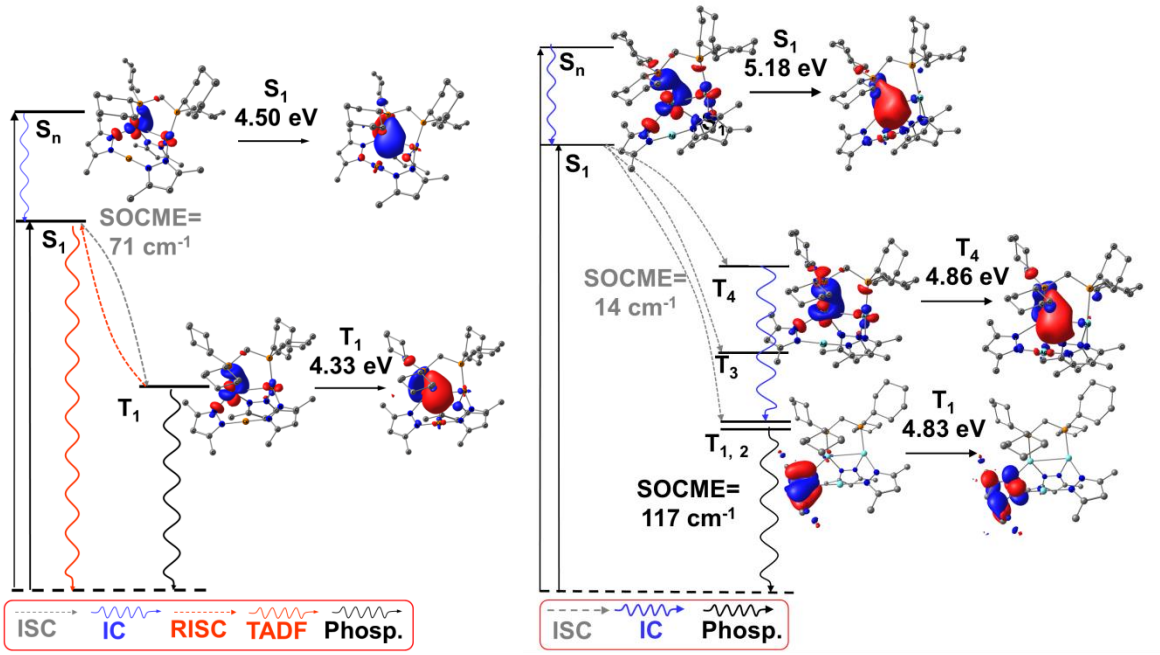

Figure 5. Schematic map of HONTO-LUNTO of the singlet and triplet excited states in the ground-state geometry and theoretically calculated energy levels, spin−orbit coupling matrix elements (SOCME, cm^{-1}) for complexes **1** (left) and **3** (right).

For the dppm-containing complexes with electron-donating pyrazoles, exemplified by {[CuL^3]$_3$(dppm)} (**8**) we found that the MC transition could occur from the T_2 exited state (0.80 fractions) (Figure 6, Table S4). This situation reflects our earlier findings for the **1*** complex,[40] where similar transition was observed from the T_5 state, while the four lowest triplets were assigned to non-radiative $^3LC^{Ph}$ (dppm phenyl substituents) transitions. Therefore, tuning of pyrazole donating properties (changing CF_3 to CH_3) allows shifting this transition to T_2, removing a large portion of $^3LC^{Ph}$ phosphorescence/non-radiative processes. Notably, **8** possesses an almost dark S_1 state (f = 0.006), while excitation to S_2 is far more effective f = 0.083. This implies that high $<S_2|T_2>$ SOC value – 223 cm^{-1} suggests competition between $S_2 \rightarrow S_1 \rightarrow T_1$ and $S_2 \rightarrow T_2 \rightarrow T_1$ processes upon excitation. The RISC process should proceed between S_1 and T_1 states with $<S_1|T_1>$ SOC=276 cm^{-1}.

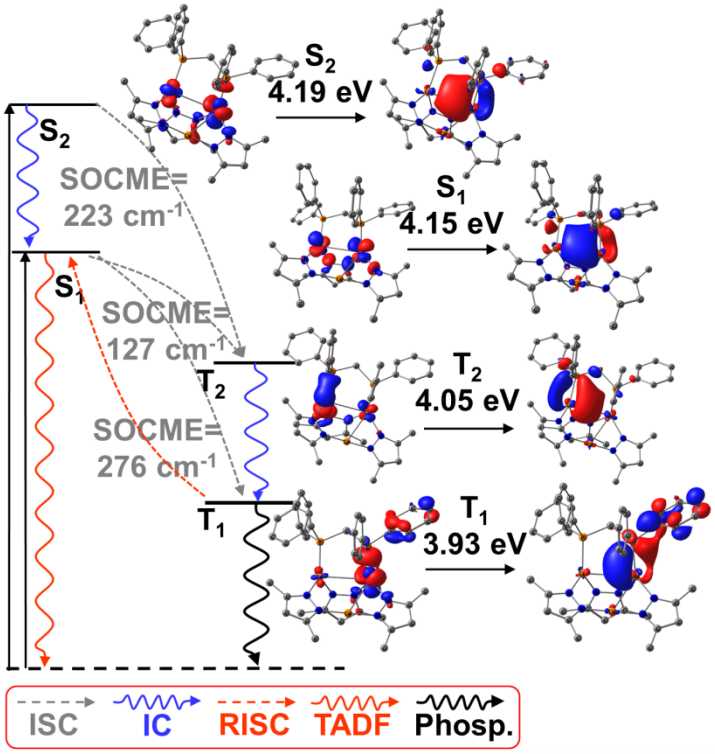

Figure 6. Schematic map of HONTO and LUNTO of the singlet and triplet excited states in the ground-state geometry and theoretically calculated energy levels, spin−orbit coupling matrix elements (SOCME, cm^{-1}) for complex **8**.

Table 5. Characteristics of lowest excited states obtained by TD-DFT.

	1	**3**	**7**	**8**
S_1 E, eV / f	4.505 / 0.044	5.176 / 0.152	4.121 / 0.027	4.155 / 0.006
S_2 E, eV / f	4.708 / 0.014	5.667 / 0.216	4.228 / 0.023	4.194 / 0.083
T_1 E, eV	4.331	4.832	3.984	3.926
T_2 E, eV	4.529	4.835	4.085	4.047
SOC T_1S_1, cm^{-1}	71	14	55	276
SOC T_2S_1, cm^{-1}	153	20	216	127
SOC T_1S_2, cm^{-1}	206	65	179	41

CONCLUSIONS

Following our strategy of decorating trinuclear silver (I) and copper (I) pyrazolates with short-bite phosphorus-containing ligands, we have overcome one of the severe drawbacks of $[ML^1]_3$(dppm) complexes – non-radiative decay from the $^3LC^{Ph}$ states of the dppm phenyl rings. By varying the substituents in the bis(phosphine)methane derivative or pyrazolate ligand, we have obtained a series of novel mixed-ligand trinuclear copper(I) and silver(I) compounds. All of the compounds exhibit similar structures in the solid state, with the planar geometry of the initial trinuclear pyrazolate complex significantly bent due to the coordination of phosphorus atoms with two metal ions.[40, 60]

The incorporation of cyclohexyl substituents in diphosphine ligands instead of phenyl ones has made possible to almost double luminescence quantum yield. Additionally, the use of more electron-donating dcpm ligand led to increased stability of the resulting complexes due to stronger metal-phosphorus bonding. The latter was also reflected by the absence of fast dynamic behavior in solution at room temperature, in contrast to the $[AgL^1]_3$ complex with a dppm ligand exhibiting "merry-go-round" motion at room temperature, which can be blocked only at 193K. The presence of more electron-donating pyrazolate ligands containing one or two methyl groups may additionally contribute to the stability of the resulting metal species.

Furthermore, the increased donicity of Me_2Pz ligand (L^3) compared to the $(CF_3)_2Pz$ (L^1) shifts the ^{3}MC excited states to the lower energies, allowing a considerable metal impact into a T_1. As a result, the mostly pure metal-centered excited state is located as an energetically accessible T_2 for $\{[CuL^3]_3(dppm)\}$, in contrast to a $\{[CuL^1]_3(dppm)\}$[40] where MC state was located only as T_5.

While higher stability of copper complexes allows the observation of luminescence in solution at room temperature, silver-containing compounds **3** and **4** are non-emissive in solution, due to non-radiative relaxation through the $^3LC^{Pz}$ states.

All copper (I) complexes feature TADF behavior in the solid state due to spin-orbit coupling between singlet and triplet metal-centered (^{3}MC) exited states, with the quantum yield up to 74%. The silver complex **3**, also shows a bathochromic shift of the emission upon cooling, which is very similar to "classic" TADF, However, numerical analysis of the lifetime versus temperature curve is not possible due to the thermal instability of the complex. Notably, this complex demonstrates unprecedented emission efficiency among all known trinuclear silver(I) pyrazolate homometallic complexes.

On the case of new mixed-ligand trinuclear copper(I) and silver(I) pyrazole-phosphine cages, we have shown the effects of substituent donating ability not only on electronic energy levels and the energy gaps between excited states but also on the efficiency of light emission. The thermally activated delayed fluorescence (TADF) behavior of copper-containing complexes provides an opportunity for using these compounds as active components in OLED devices.

EXPERIMENTAL SECTION

Physical measurement and instrumentation

^{1}H, ^{19}F and ^{31}P{^{1}H} NMR measurements were carried out on a Bruker Avance 400, FTIR spectra were collected on a Shimadzu IRPrestige 21 FT-IR spectrometer using KBr pellets.

Synthesis

No uncommon hazards are noted

Solvents (DCM, hexane, toluene) were dried by standard techniques and distilled under argon atmosphere prior to use. All operations were performed under argon atmosphere. Commercially available $Ph_2PCH_2PPh_2$ (dppm) and $Cy_2PCH_2PCy_2$ (dcpm) were used without additional purification. Initial trinuclear complexes $[ML]_3$ were obtained according literature procedures.[54]

$Cy_2PCHPhPCy_2$ ($dcpm^{Ph}$) was synthesized by the modification of previously described procedure.[61,62]

Synthesis of $dcpm^{Ph}$. To a solution of $[Cp(CO)_2Mn(\eta^2\text{-}Cy_2P{=}CHPh)](BF_4)$ (1.1 g, 2 mmol) in CH_2Cl_2 (50 mL) neat Cy_2PH (0.41 mL, 2 mmol) was added under stirring at room temperature. The color of reaction mixture changed immediately from orange to pale-yellow and IR analysis revealed the quantitative formation of $[Cp(CO)_2Mn(\kappa^1P\text{-}Cy_2PC(H)PhPCy_2H)](BF_4)$. The solution was transferred to a photochemical reactor (125 mL) by a canula, diluted with CH_2Cl_2 (50 mL) and irradiated with immersed medium pressure mercury lamp (125 W) until CO evolution ceased (*ca.* 30 min). The resulting white suspension was filtered through Celite and degassed 2M aqueous solution of NaOH (2 mL, 4 mmol) was added. After shaking the resulting yellow solution was evaporated under reduced pressure. The oily residue was dissolved in degassed toluene and rapidly purified by column chromatography on silica (2×10 cm) using toluene as an eluent. After solvent evaporation the product was recrystallized from hexane at −20°C and dried under vacuum to give $dcpm^{Ph}$ (0.7 g, 72%) as white powder.

^{1}H NMR (400 MHz, C_6D_6, 298K): δ 7.40 (br. d, $^3J_{HH}$ = 7.4 Hz, 2H, Ph), 7.14 (t overlapped with residual solvent protons, $^3J_{HH}$ = 7.7 Hz, 2H, Ph), 7.00 (t, $^3J_{HH}$ = 7.4 Hz, 1H, Ph), 3.72 (s, 1H, C*H*Ph), 2.22−2.09 (m, 4H, Cy), 2.04−1.91 (m, 4H, Cy), 1.85−1.73 (m, 6H, Cy), 1.72−1.49 (m, 12H, Cy), 1.44−1.19 (m, 12H, Cy), 1.13−0.97 (m, 6H, Cy). $^{31}P\{^1H\}$ NMR (162 MHz, C_6D_6, 25°C) : δ −4.5 (s). $^{13}C\{^1H\}$ NMR (100.6 MHz, C_6D_6, 25°C): δ 141.1 (s, $C_{ipso\ Ph}$), 129.6 (vt, J_{CP} = 5.0 Hz, $CH_{ortho\ Ph}$), 128.3 (s, $CH_{meta\ Ph}$), 125.8 (s, $CH_{para\ Ph}$), 33.6 (vt overlapped with another t signal, J_{CP} = 7.3 Hz, CH_{Cy}), 33.5 (t, $^1J_{CP}$ = 13.5 Hz, P*C*HP), 33.3 (vt, J_{CP} = 10.4 Hz, $CH_{2\ Cy}$), 31.7 (vt, J_{CP} = 8.3 Hz, $CH_{2\ Cy}$), 31.3 (vt, J_{CP} = 7.5 Hz, $CH_{2\ Cy}$), 30.2 (vt, J_{CP} = 2.8 Hz, $CH_{2\ Cy}$), 28.4

(vt, J_{CP} = 6.4 Hz, $CH_{2\ Cy}$), 28.1 (vt, J_{CP} = 2.9 Hz, $CH_{2\ Cy}$), 28.05 (vt, J_{CP} = 4.8 Hz, $CH_{2\ Cy}$), 27.9 (vt, J_{CP} = 4.9 Hz, $CH_{2\ Cy}$), 27.1 (s, $CH_{2\ Cy}$), 26.9 (s, $CH_{2\ Cy}$).

Complexes **1**-**6** were prepared according to following the procedure: an equimolar mixture of the corresponding trinuclear macrocycle (0.063 mmol) and a disphosphine (0.063mmol) was stirred overnight at room temperature in 5 ml of toluene. The solvent was evaporated to dryness under reduced pressure. The residue was dissolved in 1 mL of DCM, and then hexane (v/v = 1:3) was added to the solution. After crystallization at 5˚C the white final product was isolated by filtration.

1. Yield: 65 mg (85%) ^{1}H NMR (400 MHz, CD_2Cl_2, 298K): δ 0.88−2.03 (m, 46H, Cy + PCH_2P), 6.85 (s, 3H, CH^{Pz}). ^{19}F NMR (C_6D_6, 298 K): δ −60.2 (s, 18F, CF_3^{Pz}). ^{31}P{^{1}H} NMR (162 MHz, C_6D_6, 298 K): δ 8.83 (s). IR (KBr, cm^{-1}): 3146 (νCH^{Pz}), 2933, 2854 (νCH^{Cy}), 1640 (δCN^{Pz}) ,1256, 1118. Calc. for $Cu_3C_{40}H_{49}N_6P_2F_{18}$ (%): C, 39.67; H, 4.27; N, 6.94. Found (%): C, 39.76; H, 4.09; N, 6.95.

2. Yield : 71.2 mg (88%). ^{1}H NMR (400 MHz, CD_2Cl_2, 298K): δ 0.50−2.29 (m, 44H, Cy), 3.82 (t, $^{2}J_{PH}$ = 10.5 Hz, 1H, PCHP), 6.86 (s, 3H, CH^{Pz}), 7.17 (d, J = 6.4, 1H, CH^{Ph}), 7.32 (m, 3H, CH^{Ph}), 7.81 (d, J = 6.4, 1H, CH^{Ph}). ^{19}F NMR (400 MHz, CD_2Cl_2, 298 K): δ −59.9 (s, 18F, CF_3^{Pz}). ^{31}P{^{1}H} NMR (162 MHz, CD_2Cl_2, 298 K): δ 22.7 (s). IR (KBr, cm^{-1}): 3150 (νCH^{Pz}), 3064, 3033 (νCH^{Ph}), 2935, 2859 (νCH^{Cy}), 1633 (δCN^{Pz}), 1266, 1133. Calc. for $Cu_3C_{46}H_{53}N_6P_2F_{18}$ (%): C, 42.91; H, 4.29; N, 6.56. Found (%): C, 43.01; H, 4.16; N, 6.54.

3. Yield: 66 mg (78%) ^{1}H NMR (400 MHz, $CDCl_3$, 298 K): δ 1.01−2.01 (m, 46H, Cy + PCH_2P), 6.83 (s, 3H, CH^{Pz}). ^{19}F NMR (376.5 MHz, $CDCl_3$, 298 K): δ −60.5 (s, 18F, CF_3^{Pz}). ^{31}P{^{1}H} NMR (162 MHz, $CDCl_3$, 298 K): δ 31.00 (m, AA′XX′ system). IR (KBr, cm^{-1}): 3152

(νCH^{Pz}), 2934, 2857 (νCH^{Cy}), 1625 (δCN^{Pz}), 1261, 1130. Calc. for $Ag_3C_{40}H_{49}N_6P_2F_{18}$ (%): C, 36.02; H, 3.87; N, 6.34. Found (%): C, 35.82; H, 3.68; N, 6.27.

4. Yield : 68.3 mg (76%). ^{1}H NMR (400 MHz, $CDCl_3$, 298 K): δ 0.79−2.02 (m, 44H, Cy), 3.79 (t, $^2J_{PH}$ = 10.6 Hz, 1H, PCHP), 6.85 (s, 3H, CH^{Pz}), 7.15 (s, 1H, CH^{Ph}), 7.35 (m, 3H, CH^{Ph}), 7.65 (s, 1H, CH^{Ph}). ^{19}F NMR (376.5 MHz, $CDCl_3$, 298 K): δ −60.5 (s, 18F, CF_3^{Pz}). ^{31}P{^{1}H} NMR (162 MHz, acetone-d_6, 298 K): δ 45.45 (m, 2P, AA′XX′ system). IR (KBr, cm^{-1}): 3149 (νCH^{Pz}), 3085, 3064, 3029 (νCH^{Ph}), 2935, 2857 (νCH^{Cy}), 1261, 1130. Calc. for $Ag_3C_{46}H_{53}N_6P_2F_{18}$ (%): C, 38.81; H, 4.02; N, 5.94. Found (%): C, 38.98; H, 3.77; N, 5.93.

5. Yield: 54.1 mg (77%). ^{1}H NMR (400 MHz, $CDCl_3$, 298K): δ 1.08−2.13 (m, 46H, Cy + PCH_2P), 2.29 (s, 9H, CH_3^{Pz}), 6.45 (s, 3H, CH^{Pz}). ^{19}F NMR (376.5 MHz, $CDCl_3$, 298K): δ −58.8 (s, 9F, CF_3^{Pz}). ^{31}P{^{1}H} NMR (160 MHz, $CDCl_3$, 298 K): δ 7.23 (s). IR (KBr, cm^{-1}): 3143 (νCH^{Pz}), 2930, 2854 (νCH^{Cy}), 1630 (δCN^{Pz}), 1241, 1122. Calc. for $Cu_3C_{40}H_{58}N_6P_2F_9$ (%): C, 46.05; H, 5.65; N, 7.98. Found (%): C, 45.91; H, 5.59; N, 8.03.

6. Yield: 50.4 mg (78%). ^{1}H NMR (400 MHz, C_6D_6, 298 K): δ 2.07 (s, 9H, CH_3^{Pz}), 2.78 (t, $^2J_{PH}$ = 9.7 Hz, 2H, PCH_2P), 6.31 (s, 3H, CH^{Pz}), 6.74−6.89 (m, 12H^{Ph}), 7.20−7.31 (m, 8H^{Ph}). ^{19}F NMR (376.5 MHz, C_6D_6, 298 K): δ −59.1 (s, 9F, CF_3^{Pz}). ^{31}P{^{1}H} NMR (162 MHz, C_6D_6, 298K): δ −9.97 (s). IR (KBr, cm^{-1}): 3140 (νCH^{Pz}), 3079, 3057, 3006 (νCH^{Ph}), 2962, 2962, 2856 (νCH^{Me}), 1635 (δCN^{Pz}), 1241, 1125. Calc. for $Cu_3C_{40}H_{34}N_6P_2F_9$ (%): C, 47.18; H, 3.49; N, 8.10. Found (%): C, 46.99; H, 3.49; N, 8.22.

7. A suspension of $[CuL^3]_3$ (30 mg, 0.063 mmol) and dcpm (25.7 mg, 0.063 mmol) was stirred overnight at room temperature in 5 ml of toluene. The residue was filtered off and the solvent was evaporated to dryness under reduced pressure. The residue was dissolved in 1 mL of DCM,

and then hexane was added to the solution. After crystallization at 5˚C white product was isolated by filtration. Yield: 39.7 mg (71%). ^{1}H NMR (400 MHz, CD_2Cl_2, 298K): δ 1.06−2.09 (m, 46H, Cy), 2.25 (s, 18H, CH_3^{Pz}), 5.77 (s, 3H, CH^{Pz}). $^{31}P\{^{1}H\}$ NMR (162 MHz, CD_2Cl_2, 298 K): δ 5.1 (s). IR (KBr, cm^{-1}): 3100 (νCH^{Pz}), 2927, 2850 (νCH^{Cy}+ νCH^{Me}), 1640 (δCN^{Pz}), 1450, 1263. Calc. for $Cu_3C_{40}H_{67}N_6P_2$ (%): C, 54.56; H, 7.88; N, 9.35. Found (%): C, 54.31; H, 7.63; N, 9.50.

8. Complex was similarly prepared according to the procedure for **7** using dppm as a ligand (24.2 mg, 0.063 mmol). Yield: 39.7 mg (73%). ^{1}H NMR (400 MHz, CD_2Cl_2, 298 K): δ 2.20 (s, 18H, CH_3^{Pz}), 3.26 (t, $^{2}J_{PH}$ = 8.5 Hz, 2H, PCH_2P), 5.85 (s, 3H, CH^{Pz}), 7.16−7.67 (m, 20H, CH^{Ph}). $^{31}P\{^{1}H\}$ NMR (162 MHz, CD_2Cl_2, 298 K): δ −14.8 (s). IR (KBr, cm^{-1}): 3104 (νCH^{Pz}), 3071, 3053, 3020 (νCH^{Ph}), 2938, 2908, 2854 (νCH^{Me}), 1522, 1435, 1345, 1100. Calc. for $Cu_3C_{40}H_{43}N_6P_2$ (%): C, 55.96; H, 5.16; N, 9.80. Found (%): C, 55.84; H, 5.04; N, 9.77.

Photophysical measurements

Helium-nitrogen optical cryostat optCryo 105-40 with temperature control system were used for the samples cooling in the range of temperatures 295 – 77 K. Heating of the samples (310 – 340 K) was performed by using a Quantum Northwest Qpod-2e cuvette sample compartment. Emission spectra of complexes in solution and solid state were measured using a DTL–375QT pulse laser (wavelength 355 nm, pulse width 5 ns, repetition frequency 10 − 1000 Hz) or TECH-263 Basic pulse laser (wavelength 263 nm, pulse width 5 ns, repetition frequency 10 − 1000 Hz) as an excitation source and an Avantes AvaSpec-2048x64 spectrometer. An Ocean Optics monochromator (Monoscan-2000, interval of wavelengths 1 nm), a FASTComTec (MCS6A1T4) multiple-event time digitizer, a Hamamatsu (H10682-01) photon counting head were used for lifetime measurements. The steady-state excitation spectra of complexes in the solid state and

solution at 298 K and 77 K were recorded on a FluoroMax 4 and a FluoroLog 3 Horiba spectrofluorometers. The Xenon lamps (300 W and 450 W) were used as excitation sources. The absolute emission quantum yields of the crystalline samples were determined on a FluoroLog 3 Horiba spectrofluorometer equipped with a Quanta-phi integration sphere.

Computational details.

Calculations were performed with ORCA 5.04 software package[63-64] applying ωB97X-D3 functional[65] and ZORA Hamiltonian. The applied basis set was SARC-ZORA-TZVPP[66] for silver atoms and ZORA-TZVPP for H, C, N, F and Cu atoms. Electronic transitions were calculated under the TD-DFT approach utilizing the same computation level as the Tamm-Dankoff approximation taking into account 20 lowest energy singlet and triplet excitations. Analysis of natural transition orbitals (NTO) and contributions from certain atomic orbitals to the electronic transitions were performed with the Multiwfn 3.8 package[67]. For the complexation energy analysis methodology previously used in was applied. Optimizations of the complexes geometries were performed by the ADF2014[68] software suit utilizing BP86 functional with Grimme D3 correction[69] and TZ2P basis set. With the EDA[70-72] approach, the fragments interaction energy, ΔE_{int}, was decomposed into terms $\Delta E_{int} = \Delta E_{elstat} + \Delta E_{Pauli} + \Delta E_{orb} + \Delta E_{disp}$. ΔE_{orb} was further decomposed with ETS-NOCV approach to the electron density transfer channels, $\Delta\rho_i(r)$.[73] The energy of complex formation was determined as $\Delta E_{total} = \Delta E_{int} + \Delta E_{prep}$, where ΔE_{prep} is energy of deformation of fragments (dppm and $[ML]_3$) from free "relaxed" state to their state in the complex. These data provided in the TableS1

SC-XRD study

Single-crystal X-ray diffraction experiments of complexes were carried out with a Bruker APEX-II diffractometer at 120K using MoKα source (λ = 0.71073). The APEX II software[74] was used for collecting frames of data, indexing reflections, determination of

lattice constants, integration of intensities of reflections, scaling, and absorption correction. All structures were solved by dual-space algorithm embedded in ShelXT[75] and refined in anisotropic approximation for non-hydrogen atoms against F^2 (*hkl*) using the ShelXL[76] program. Hydrogen atoms of aromatic fragments were calculated according to those idealized geometry and refined with constraints applied to C-H bond lengths and equivalent displacement parameters (Ueq (H) = 1.2Ueq (X), X - cental atom of XH_2 group; Ueq (H) = 1.5U eq (Y), Y - central atom of YH_3 group). Molecular graphics was drawn using OLEX2[77] program.

ASSOCIATED CONTENT

Supporting Information

The Supporting Information containing NMR, FTIR, UV-vis and photoluminescence spectra, detailed results of DFT and TDDFT calculations, and crystal data for complexes **1-4**, **6**, **7** is available free of charge on the ACS Publications website.

Accession Codes

CCDC 2333924-2333929 contain the supplementary crystallographic data for this paper. These data can be obtained free of charge via www.ccdc.cam.ac.uk/data_request/cif.

AUTHOR INFORMATION

Corresponding Author

* E.S.S. e-mail: shu@ineos.ac.ru

* S.P.T. e-mail: sergey.tunik@spbu.ru

Notes

The authors declare no competing financial interest.

ACKNOWLEDGMENT

The synthetic and structural studies were funded by the Russian Science Foundation, grant number 22-73-10130. The photophysical studies were funded by the Russian Science Foundation, project 19-73-20055-П. The work was performed using the equipment of the Research Park of St. Petersburg State University (Centers for Optical and Laser Materials Research). The elemental analysis was performed employing the equipment of the Center for Molecular Composition Studies of INEOS RAS with support from the Ministry of Science and Higher Education of the Russian Federation.

[§]Dedication: In commemoration of the 300th anniversary of St Petersburg State University and 70th anniversary of A. N. Nesmeyanov Institute of Organoelement Compounds.

REFERENCES

1. Yam, V. W.-W.; Au, V. K.-M.; Leung, S. Y.-L., Light-Emitting Self-Assembled Materials Based on d8 and d10 Transition Metal Complexes. *Chem. Rev.* **2015**, *115*, 7589-7728.

2. Herrera, R. P.; Gimeno, M. C., Main Avenues in Gold Coordination Chemistry. *Chem. Rev.* **2021**, *121*, 8311-8363.

3. Li, X.; Xie, Y.; Li, Z., Diversity of Luminescent Metal Complexes in OLEDs: Beyond Traditional Precious Metals. *Asian J. Chem.* **2021**, *16*, 2817-2829.

4. Volz, D.; Wallesch, M.; Flechon, C.; Danz, M.; Verma, A.; Navarro, J. M.; Zink, D. M.; Brase, S.; Baumann, T., From iridium and platinum to copper and carbon: new avenues for more sustainability in organic light-emitting diodes. *Green. Chem.* **2015**, *17*, 1988-2011.

5. Di, D.; Romanov, A. S.; Yang, L.; Richter, J. M.; Rivett, J. P.; Jones, S.; Thomas, T. H.; Abdi Jalebi, M.; Friend, R. H.; Linnolahti, M.; Bochmann, M.; Credgington, D., High-performance light-emitting diodes based on carbene-metal-amides. *Science* **2017**, *356*, 159-163.

6. Fresta, E.; Costa, R. D., Beyond traditional light-emitting electrochemical cells – a review of new device designs and emitters. *J. Mater. Chem. C* **2017**, *5*, 5643-5675.

7. Bizzarri, C.; Spuling, E.; Knoll, D. M.; Volz, D.; Bräse, S., Sustainable metal complexes for organic light-emitting diodes (OLEDs). *Coord. Chem. Rev.* **2018**, *373*, 49-82.

8. Ravaro, L. P.; Zanoni, K. P. S.; de Camargo, A. S. S., Luminescent Copper(I) complexes as promising materials for the next generation of energy-saving OLED devices. *Energy Reports* **2020**, *6*, 37-45.

9. Keller, S.; Prescimone, A.; La Placa, M. G.; Junquera-Hernandez, J. M.; Bolink, H. J.; Constable, E. C.; Sessolo, M.; Orti, E.; Housecroft, C. E., The shiny side of copper: bringing copper(I) light-emitting electrochemical cells closer to application. *RSC Adv.* **2020**, *10*, 22631-22644.

10. Hernandez-Perez, A. C.; Collins, S. K., Heteroleptic Cu-Based Sensitizers in Photoredox Catalysis. *Acc. Chem. Res.* **2016**, *49*, 1557-1565.

11. Cheung, K. P. S.; Sarkar, S.; Gevorgyan, V., Visible Light-Induced Transition Metal Catalysis. *Chem. Rev.* **2022**, *122*, 1543-1625.

12. Muniz, C. N.; Archer, C. A.; Applebaum, J. S.; Alagaratnam, A.; Schaab, J.; Djurovich, P. I.; Thompson, M. E., Two-Coordinate Coinage Metal Complexes as Solar Photosensitizers. *J. Am. Chem. Soc.* **2023**, *145*, 13846-13857.

13. Peng, Y.; Bao, H.; Zheng, L.; Zhou, Y.; Ni, Q.; Chen, X.; Li, Y.; Yan, P.; Yang, Y. F.; Liu, Y., Cu(I)-Photosensitizer-Catalyzed Olefin-alpha-Amino Radical Metathesis/Demethylenative Cyclization of 1,7-Enynes. *Org. Lett.* **2024**, *26*, 3218-3223.

14. Lu, X.; Wei, S.; Wu, C.-M. L.; Li, S.; Guo, W., Can Polypyridyl Cu(I)-based Complexes Provide Promising Sensitizers for Dye-Sensitized Solar Cells? A Theoretical Insight into Cu(I) versus Ru(II) Sensitizers. *J. Phys.Chem.C* **2011**, *115*, 3753-3761.

15. Bozic-Weber, B.; Constable, E. C.; Housecroft, C. E., Light harvesting with Earth abundant d-block metals: Development of sensitizers in dye-sensitized solar cells (DSCs). *Coord. Chem. Rev.* **2013**, *257*, 3089-3106.

16. Franchi, D.; Leandri, V.; Pizzichetti, A. R. P.; Xu, B.; Hao, Y.; Zhang, W.; Sloboda, T.; Svanstrom, S.; Cappel, U. B.; Kloo, L.; Sun, L.; Gardner, J. M., Effect of the Ancillary Ligand on the Performance of Heteroleptic Cu(I) Diimine Complexes as Dyes in Dye-Sensitized Solar Cells. *ACS Appl. Energy Mater.* **2022**, *5*, 1460-1470.

17. Beaudelot, J.; Oger, S.; Perusko, S.; Phan, T. A.; Teunens, T.; Moucheron, C.; Evano, G., Photoactive Copper Complexes: Properties and Applications. *Chem Rev* **2022,** *122* (22), 16365-16609.

18. Hsu, C. W.; Lin, C. C.; Chung, M. W.; Chi, Y.; Lee, G. H.; Chou, P. T.; Chang, C. H.; Chen, P. Y., Systematic investigation of the metal-structure-photophysics relationship of emissive d10-complexes of group 11 elements: the prospect of application in organic light emitting devices. *J. Am. Chem. Soc.* **2011**, *133*, 12085-12099.

19. Shafikov, M. Z.; Czerwieniec, R.; Yersin, H., Ag(i) complex design affording intense phosphorescence with a landmark lifetime of over 100 milliseconds. *Dalton Trans.* **2019**, *48*, 2802-2806.

20. Shafikov, M. Z.; Suleymanova, A. F.; Czerwieniec, R.; Yersin, H., Design Strategy for Ag(I)-Based Thermally Activated Delayed Fluorescence Reaching an Efficiency Breakthrough. *Chem. Mater.* **2017**, *29*, 1708-1715.

21. Shafikov, M. Z.; Suleymanova, A. F.; Czerwieniec, R.; Yersin, H., Thermally Activated Delayed Fluorescence from Ag(I) Complexes: A Route to 100% Quantum Yield at Unprecedentedly Short Decay Time. *Inorg. Chem.* **2017**, *56*, 13274-13285.

22. Artem'ev, A. V.; Shafikov, M. Z.; Schinabeck, A.; Antonova, O. V.; Berezin, A. S.; Bagryanskaya, I. Y.; Plusnin, P. E.; Yersin, H., Sky-blue thermally activated delayed fluorescence (TADF) based on Ag(i) complexes: strong solvation-induced emission enhancement. *Inorg. Chem. Front.* **2019,** *6*, 3168-3176.

23. Chakkaradhari, G.; Eskelinen, T.; Degbe, C.; Belyaev, A.; Melnikov, A. S.; Grachova, E. V.; Tunik, S. P.; Hirva, P.; Koshevoy, I. O., Oligophosphine-thiocyanate Copper(I) and Silver(I) Complexes and Their Borane Derivatives Showing Delayed Fluorescence. *Inorg. Chem.* **2019,** *58*, 3646-3660.

24. Beliaeva, M.; Belyaev, A.; Grachova, E. V.; Steffen, A.; Koshevoy, I. O., Ditopic Phosphide Oxide Group: A Rigidifying Lewis Base to Switch Luminescence and Reactivity of a Disilver Complex. *J. Am. Chem. Soc.* **2021**, *143*, 15045-15055.

25. Dias, H. V. R.; Diyabalanage, H. V. K.; Ghimire, M. M.; Hudson, J. M.; Parasar, D.; Palehepitiya Gamage, C. S.; Li, S.; Omary, M. A., Brightly phosphorescent tetranuclear copper(I) pyrazolates. *Dalton Trans.* **2019**, *48*, 14979-14983.

26. Li, J.; Wang, L.; Zhao, Z.; Li, X.; Yu, X.; Huo, P.; Jin, Q.; Liu, Z.; Bian, Z.; Huang, C., Two-Coordinate Copper(I)/NHC Complexes: Dual Emission Properties and Ultralong Room-Temperature Phosphorescence. *Angew. Chem. Int. Ed.* **2020**, *59*, 8210-8217.

27. Ma, X. H.; Si, Y.; Hu, J. H.; Dong, X. Y.; Xie, G.; Pan, F.; Wei, Y. L.; Zang, S. Q.; Zhao, Y., High-Efficiency Pure Blue Circularly Polarized Phosphorescence from Chiral N-Heterocyclic-Carbene-Stabilized Copper(I) Clusters. *J. Am. Chem. Soc.* **2023**, *145*, 25874-25886.

28. Czerwieniec, R.; Leitl, M. J.; Homeier, H. H. H.; Yersin, H., Cu(I) complexes – Thermally activated delayed fluorescence. Photophysical approach and material design. *Coord. Chem. Rev.* **2016**, *325*, 2-28.

29. Housecroft, C. E.; Constable, E. C., TADF: Enabling luminescent copper(i) coordination compounds for light-emitting electrochemical cells. *J. Mater. Chem.* **2022**, *10*, 4456-4482.

30. Artem'ev, A. V.; Demyanov, Y. V.; Rakhmanova, M. I.; Bagryanskaya, I. Y., Pyridylarsine-based Cu(I) complexes showing TADF mixed with fast phosphorescence: a speeding-up emission rate using arsine ligands. *Dalton Trans.* **2022**, *51*, 1048-1055.

31. Li, T.-y.; Schaab, J.; Djurovich, P. I.; Thompson, M. E., Toward rational design of TADF two-coordinate coinage metal complexes: understanding the relationship between natural transition orbital overlap and photophysical properties. *J. Mater. Chem. C* **2022,** *10*, 4674-4683.

32. Yersin, H.; Czerwieniec, R.; Monkowius, U.; Ramazanov, R.; Valiev, R.; Shafikov, M. Z.; Kwok, W.-M.; Ma, C., Intersystem crossing, phosphorescence, and spin-orbit coupling. Two contrasting Cu(I)-TADF dimers investigated by milli- to micro-second phosphorescence, femto-second fluorescence, and theoretical calculations. *Coord. Chem. Rev.* **2023**, *478*.

33. Baranov, A. Y.; Rakhmanova, M. I.; Hei, X.; Samsonenko, D. G.; Stass, D. V.; Bagryanskaya, I. Y.; Ryzhikov, M. R.; Fedin, V. P.; Li, J.; Artem'ev, A. V., A new subclass of copper(I) hybrid emitters showing TADF with near-unity quantum yields and a strong solvatochromic effect. *Chem. Commun.* **2023**, *59*, 2923-2926.

34. Yersin, H.; Czerwieniec, R.; Shafikov, M. Z.; Suleymanova, A. F., TADF Material Design: Photophysical Background and Case Studies Focusing on Cu(I) and Ag(I) Complexesa. In *Highly Efficient OLEDs: Materials Based on Thermally Activated Delayed Fluorescence*, Yersin, H., Ed. 2018; 1-60.

35. Lipinski, S.; Cavinato, L. M.; Pickl, T.; Biffi, G.; Pöthig, A.; Coto, P. B.; Fernández-Cestau, J.; Costa, R. D., Dual-Phosphorescent Heteroleptic Silver(I) Complex in Long-Lasting Red Light-Emitting Electrochemical Cells. *Adv. Opt. Mater.* **2023**, *11*, 2203145.

36. Titova, E. M.; Titov, A. A.; Shubina, E. S., Functional pyrazolylpyridine ligands in the design of metal complexes with tunable properties. *Russ. Chem. Rev.* **2023**, *92*, RCR5099.

37. Titov, A. A.; Filippov, O. A.; Epstein, L. M.; Belkova, N. V.; Shubina, E. S., Macrocyclic copper(I) and silver(I) pyrazolates: Principles of supramolecular assemblies with Lewis bases. *Inorg. Chim. Acta* **2018**, *470*, 22-35.

38. Zheng, J.; Lu, Z.; Wu, K.; Ning, G. H.; Li, D., Coinage-Metal-Based Cyclic Trinuclear Complexes with Metal-Metal Interactions: Theories to Experiments and Structures to Functions. *Chem. Rev.* **2020**, *120*, 9675-9742.

39. Watanabe, Y.; Washer, B. M.; Zeller, M.; Savikhin, S.; Slipchenko, L. V.; Wei, A., Copper(I)-Pyrazolate Complexes as Solid-State Phosphors: Deep-Blue Emission through a Remote Steric Effect. *J. Am. Chem. Soc.* **2022**, *144*, 10186-10192.

40. Titov, A. A.; Filippov, O. A.; Smol'yakov, A. F.; Godovikov, I. A.; Shakirova, J. R.; Tunik, S. P.; Podkorytov, I. S.; Shubina, E. S., Luminescent Complexes of the Trinuclear Silver(I) and Copper(I) Pyrazolates Supported with Bis(diphenylphosphino)methane. *Inorg. Chem.* **2019**, *58*, 8645-8656.

41. Titov, A. A.; Filippov, O. A.; Smol'yakov, A. F.; Averin, A. A.; Shubina, E. S., Synthesis, structures and luminescence of multinuclear silver(i) pyrazolate adducts with 1,10-phenanthroline derivatives. *Dalton Trans.* **2019**, *48*, 8410-8417.

42. Lakhi, J. S.; Patterson, M. R.; Dias, H. V. R., Coinage metal metallacycles involving a fluorinated 3,5-diarylpyrazolate. *New. J. Chem.* **2020**, *44*, 14814-14822.

43. Emashova, S. K.; Titov, A. A.; Smol'yakov, A. F.; Chernyadyev, A. Y.; Godovikov, I. A.; Godovikova, M. I.; Dorovatovskii, P. V.; Korlykov, A. A.; Filippov, O. A.; Shubina, E. S., Emissive silver(i) cyclic trinuclear complexes with aromatic amine donor pyrazolate derivatives: way to efficiency. *Inorg. Chem. Front.* **2022**, *9*, 5624-5634.

44. Dias, H. V.; Gamage, C. S., Arene-sandwiched silver(I) pyrazolates. *Angew. Chem. Int. Ed.* **2007**, *46*, 2192-2194.

45. Jayaratna, N. B.; Cowan, M. G.; Parasar, D.; Funke, H. H.; Reibenspies, J.; Mykhailiuk, P. K.; Artamonov, O.; Noble, R. D.; Dias, H. V. R., Low Heat of Adsorption of Ethylene Achieved by Major Solid-State Structural Rearrangement of a Discrete Copper(I) Complex. *Angew. Chem. Int. Ed.* **2018**, *130*, 16680-16684.

46. Titov, A. A.; Larionov, V. A.; Smol'yakov, A. F.; Godovikova, M. I.; Titova, E. M.; Maleev, V. I.; Shubina, E. S., Interaction of a trinuclear copper(I) pyrazolate with alkynes and carbon-carbon triple bond activation. *Chem. Commun.* **2019**, *55*, 290-293.

47. Parasar, D.; Ponduru, T. T.; Noonikara-Poyil, A.; Jayaratna, N. B.; Dias, H. V. R., Acetylene and terminal alkyne complexes of copper(I) supported by fluorinated pyrazolates: syntheses, structures, and transformations. *Dalton Trans.* **2019**, *48*, 15782-15794.

48. Xu, J.-P.; Zou, W.; Zhan, S.-Z.; Zheng, J.; Wu, K.; Zhang, G.-H.; Li, J.-H.; Li, M.; Ning, G.-H.; Li, D., Visible-light excited luminescent trigonal prismatic metallocages from a template-directed assembly. *Inorg. Chem. Front.* **2021**, *8*, 3222-3229.

49. Song, J.-G.; Zheng, J.; Wei, R.-J.; Huang, Y.-L.; Jiang, J.; Ning, G.-H.; Wang, Y.; Lu, W.; Ye, W.-C.; Li, D., Crystalline mate for structure elucidation of organic molecules. *Chem* **2024**, *10*, 924-937.

50. Chen, J. H.; Liu, Y. M.; Zhang, J. X.; Zhu, Y. Y.; Tang, M. S.; Ng, S. W.; Yang, G., Halogen-involving weak interactions manifested in the crystal structures of silver(I) or gold(I) 4-halogenated-3,5-diphenylpyrazolato trimers. *Crystengcomm.* **2014**, *16*, 4987-4998.

51. Zhan, S. Z.; Chen, W.; Zheng, J.; Ng, S. W.; Li, D., Luminescent polymorphic aggregates of trinuclear Cu(I)-pyrazolate tuned by intertrimeric CuNPy weak coordination bonds. *Dalton Trans.* **2021**, *50*, 1733-1739.

52. Tang, W.-J.; Yang, H.; Peng, S.-K.; Xiao, Z.-M.; Huang, G.-Q.; Zheng, J.; Li, D., Multistimuli-responsive behavior of a phosphorescent Cu3pyrazolate3 complex for luminescent logic gates and encrypted information transformation. *Inorg. Chem. Front.* **2023**, *10*, 2594-2606.

53. Dias, H. V. R.; Diyabalanage, H. V. K.; Rawashdeh-Omary, M. A.; Franzman, M. A.; Omary, M. A., Bright Phosphorescence of a Trinuclear Copper(I) Complex: Luminescence Thermochromism, Solvatochromism, and "Concentration Luminochromism". *J. Am. Chem. Soc.* **2003**, *125*, 12072-12073.

54. Dias, H. V.; Diyabalanage, H. V.; Eldabaja, M. G.; Elbjeirami, O.; Rawashdeh-Omary, M. A.; Omary, M. A., Brightly phosphorescent trinuclear copper(I) complexes of pyrazolates: substituent effects on the supramolecular structure and photophysics. *J. Am. Chem. Soc.* **2005,** *127*, 7489-501.

55. Omary, M. A.; Rawashdeh-Omary, M. A.; Gonser, M. W. A.; Elbjeirami, O.; Grimes, T.; Cundari, T. R.; Diyabalanage, H. V. K.; Gamage, C. S. P.; Dias, H. V. R., Metal Effect on the Supramolecular Structure, Photophysics, and Acid−Base Character of Trinuclear Pyrazolato Coinage Metal Complexes. *Inorg. Chem.* **2005**, *44*, 8200-8210.

56. El Sayed Moussa, M.; Evariste, S.; Wong, H. L.; Le Bras, L.; Roiland, C.; Le Polles, L.; Le Guennic, B.; Costuas, K.; Yam, V. W. W.; Lescop, C., A solid state highly emissive Cu(I) metallacycle: promotion of cuprophilic interactions at the excited states. *Chem. Commun.* **2016**, *52*, 11370-11373.

57. He, L. H.; Luo, Y. S.; Di, B. S.; Chen, J. L.; Ho, C. L.; Wen, H. R.; Liu, S. J.; Wang, J. Y.; Wong, W. Y., Luminescent Three- and Four-Coordinate Dinuclear Copper(I) Complexes Triply Bridged by Bis(diphenylphosphino)methane and Functionalized 3-(2'-Pyridyl)-1,2,4-triazole Ligands. *Inorg. Chem.* **2017**, *56*, 10311-10324.

58. Yersin, H.; Czerwieniec, R.; Shafikov, M. Z.; Suleymanova, A. F., TADF Material Design: Photophysical Background and Case Studies Focusing on CuI and AgI Complexes. *ChemPhysChem* **2017**, *18*, 3508-3535.

59. Artem'ev, A. V.; Doronina, E. P.; Rakhmanova, M. I.; Hei, X.; Stass, D. V.; Tarasova, O. A.; Bagryanskaya, I. Y.; Samsonenko, D. G.; Novikov, A. S.; Nedolya, N. A.; Li, J., A family of CuI-based 1D polymers showing colorful short-lived TADF and phosphorescence induced by photo- and X-ray irradiation. *Dalton Trans.* **2023**, *52*, 4017-4027.

60. Filippov, O. A.; Titov, A. A.; Guseva, E. A.; Loginov, D. A.; Smol'yakov, A. F.; Dolgushin, F. M.; Belkova, N. V.; Epstein, L. M.; Shubina, E. S., Remarkable Structural and Electronic Features of the Complex Formed by Trimeric Copper Pyrazolate with Pentaphosphaferrocene. *Eur. J. Chem.* **2015**, *21*, 13176-13180.

61. Valyaev, D. A.; Bastin, S.; Utegenov, K. I.; Lugan, N.; Lavigne, G.; Ustynyuk, N. A., A direct, modular, and efficient construction of the P-C-P structural motif through coupling of manganese carbyne complexes with phosphines. *Eur. J. Chem.* **2014**, *20*, 2175-8.

62. Valyaev, D. A.; Filippov, O. A.; Lugan, N.; Lavigne, G.; Ustynyuk, N. A., Umpolung of Methylenephosphonium Ions in Their Manganese Half-Sandwich Complexes and Application to the Synthesis of Chiral Phosphorus-Containing Ligand Scaffolds. *Angew. Chem. Int. Ed.* **2015**, *127*, 6413-6417.

63. Neese, F., The ORCA program system. *WIREs Comput. Mol. Sci.*, 2011, 2, 73-78.

64. Neese, F., Software update: The ORCA program system—Version 5.0. *WIREs Comput. Mol. Sci.*, **2022**, *1*, e1606.

65. Lin, Y. S.; Li, G. D.; Mao, S. P.; Chai, J. D., Long-Range Corrected Hybrid Density Functionals with Improved Dispersion Corrections. *J. Chem. Theory Comput.* **2013,** *9*, 263-72.

66. Rolfes, J. D.; Neese, F.; Pantazis, D. A., All-electron scalar relativistic basis sets for the elements Rb-Xe. *J. Comput. Chem.* **2020**, *41*, 1842-1849.

67. Lu, T.; Chen, F., Multiwfn: a multifunctional wavefunction analyzer. *J. Comput. Chem.* **2012**, *33*, 580-592.

68. Baerends, E. J.; Ziegler, T.; Autschbach, J.; Bashford, D.; Bérces, A.; Bickelhaupt, F. M.; Bo, C.; Boerrigter, P. M.; Cavallo, L.; Chong, D. P.; Deng, L.; Dickson, R. M.; Ellis, D. E.; van Faassen, M.; Fan, L.; Fischer, T. H.; Fonseca Guerra, C.; Ghysels, A.; Giammona, A.; van Gisbergen, S. J. A.; Götz, A. W.; Groeneveld, J. A.; Gritsenko, O. V.; Grüning, M.; Gusarov, S.; Harris, F. E.; van den Hoek, P.; Jacob, C. R.; Jacobsen, H.; Jensen, L.; Kaminski, J. W.; van Kessel, G.; Kootstra, F.; Kovalenko, A.; Krykunov, M. V.; van Lenthe, E.; McCormack, D. A.; Michalak, A.; Mitoraj, M.; Neugebauer, J.; Nicu, V. P.; Noodleman, L.; Osinga, V. P.; Patchkovskii, S.; Philipsen, P. H. T.; Post, D.; Pye, C. C.; Ravenek, W.; Rodríguez, J. I.; Ros, P.; Schipper, P. R. T.; Schreckenbach, G.; Seldenthuis, J. S.; Seth, M.; Snijders, J. G.; Solà, M.; Swart, M.; Swerhone, D.; te Velde, G.; Vernooijs, P.; Versluis, L.; Visscher, L.; Visser, O.; Wang, F.; Wesolowski, T. A.; van Wezenbeek, E. M.; Wiesenekker, G.; Wolff, S. K.; Woo, T. K.; Yakovlev, A. L. *ADF2014*, SCM, Theoretical Chemistry, Vrije Universiteit: Amsterdam, The Netherlands.

69. Grimme, S.; Ehrlich, S.; Goerigk, L., Effect of the damping function in dispersion corrected density functional theory. *J. Comput. Chem.* **2011**, *32*, 1456-1465.

70. Ziegler, T.; Rauk, A., A theoretical study of the ethylene-metal bond in complexes between copper(1+), silver(1+), gold(1+), platinum(0) or platinum(2+) and ethylene, based on the Hartree-Fock-Slater transition-state method. *Inorg. Chem.* **1979**, *18*, 1558-1565.

71. Ziegler, T.; Rauk, A., Carbon monoxide, carbon monosulfide, molecular nitrogen, phosphorus trifluoride, and methyl isocyanide as .sigma. donors and .pi. acceptors. A theoretical study by the Hartree-Fock-Slater transition-state method. *Inorg. Chem.* **1979**, *18*, 1755-1759.

72. Bickelhaupt, F. M.; Baerends, E. J., Kohn-Sham Density Functional Theory: Predicting and Understanding Chemistry. In *Reviews in Computational Chemistry*, Lipkowitz, K. B.; Boyd, D. B., Eds. John Wiley & Sons, Inc.: 2007; Vol. 15, pp 1-86.

73. Mitoraj, M. P.; Michalak, A.; Ziegler, T., A Combined Charge and Energy Decomposition Scheme for Bond Analysis. *J. Chem. Theory Comput.* **2009**, *5*, 962-975.

74. *APEX II software package; Bruker AXS Inc.: 5465, East Cheryl Parkway, Madison, WI 5317, 2005.*

75. Sheldrick, G., SHELXT - Integrated space-group and crystal-structure determination. *Acta Crystallogr. Sect. A*, 2015, **71**, 3-8.

76. Sheldrick, G., Crystal structure refinement with SHELXL. *Acta Crystallogr., Sect. C.*, 2015, **71**, 3-8.

77. Dolomanov, O. V.; Bourhis, L. J.; Gildea, R. J.; Howard, J. A. K.; Puschmann, H., OLEX2: a complete structure solution, refinement and analysis program. *J. Appl. Crystallogr.* **2009,** *42*, 339-341.